Propagation of positional error in 3D GIS: estimation of the solar irradiation of building roofs

Filip Biljecki *
3D Geoinformation, Delft University of Technology, The Netherlands
Gerard B.M. Heuvelink
Soil Geography and Landscape group, Wageningen University, Wageningen, The Netherlands
Hugo Ledoux
3D Geoinformation, Delft University of Technology, The Netherlands
Jantien Stoter
3D Geoinformation, Delft University of Technology, The Netherlands

ORCID

FB: http://orcid.org/0000-0002-6229-7749
GH: http://orcid.org/0000-0003-0959-9358
HL: http://orcid.org/0000-0002-1251-8654
JS: http://orcid.org/0000-0002-1393-7279

* Corresponding author at f.biljecki@tudelft.nl

This is an Accepted Manuscript of an article published by Taylor & Francis in the journal *International Journal of Geographical Information Science*, available online:
http://doi.org/10.1080/13658816.2015.1073292

Cite as:

Biljecki, F., Heuvelink, G. B. M., Ledoux, H., and Stoter, J. (2015): Propagation of positional error in 3D GIS: estimation of the solar irradiation of building roofs. *International Journal of Geographical Information Science*, vol. 29(12), pp. 2269-2294.

Abstract

While error propagation in GIS is a topic that has received a lot of attention, it has not been researched with 3D GIS data. We extend error propagation to 3D city models by using a Monte Carlo simulation on a use case of annual solar irradiation estimation of building rooftops for assessing the efficiency of installing solar panels. Besides investigating the extension of the theory of error propagation in GIS from 2D to 3D, this paper presents the following contributions. We (1) introduce varying XY/Z accuracy levels of the geometry to reflect actual acquisition outcomes; (2) run experiments on multiple accuracy classes (121 in total); (3) implement an uncertainty engine for simulating acquisition positional errors to procedurally modelled (synthetic) buildings; (4) perform the uncertainty propagation analysis on multiple levels of detail (LODs); and (5) implement Solar3Dcity—a CityGML compliant software for estimating the solar irradiation of roofs, which we use in our experiments. The results show that in the case of the city of Delft in the Netherlands, a 0.3/0.6 m positional uncertainty yields an error of 68 kWh/m^2/year (10%) in solar irradiation estimation. Further, the results indicate that the planar and vertical uncertainty have a different influence on the estimations, and that the results are comparable between LODs. In the experiments we use procedural models, which implies that analyses are done in a controlled environment where results can be validated. Our uncertainty propagation method and the framework are applicable to other 3D GIS operations and/or use cases. We released Solar3Dcity as open-source software to support related research efforts in the future.

Keywords: Error propagation; uncertainty; CityGML; 3D GIS; photovoltaic potential

1 Introduction

The acquisition and utilisation of geographic information go together with errors. Error propagation in GIS refers both to the unavoidable erroneous nature of processing and utilising GIS datasets, and to a field of research that investigates the propagation of errors in the input to a GIS operation to the errors in its output (Heuvelink, 2005; Lemmens, 2011).

Two common methods to determine the propagation of errors through GIS operations are the Taylor series method and the Monte Carlo method (Xue *et al.*, 2015). The former is analytical and establishes mathematical functions that portray the uncertainty propagation, while the latter is a numerical simulation method. Many GIS analyses are too complex to be solved analytically, hence the Monte Carlo method is frequently used (Yeh and Li, 2006).

While error propagation is a mature and much studied subject in geoinformation science, research has essentially been limited to 2D situations. The only exception that we know of being a recent introductory work by Biljecki *et al.* (2014a). Further, recent work is focused towards raster data and attribute uncertainty, and research on vector data and positional uncertainty are less common. Extending the error propagation problem from 2D to 3D is more complex than one may expect, which motivated us to research this topic in 3D.

The foundations of error propagation are valid for any dimension, however, in the context of 3D city models there are several factors to take into account:

(1) *Combination of multiple acquisition techniques and accuracy levels*. In contrast to 2D data, a significant number of 3D city models is produced with a combination of multiple acquisition techniques, such as photogrammetry (Suveg and Vosselman, 2004), LiDAR (Vosselman and Dijkman, 2001; Tomljenovic *et al.*, 2015), extrusion from 2D data (Ledoux and Meijers, 2011), and as a generalised conversion from Building Information Models (BIM) (Isikdag and Zlatanova, 2009; Donkers *et al.*, 2015). Since a model may be constructed using multiple techniques that each have different accuracy levels, this results in different positional accuracy for the x, y coordinates on the one hand, and the z coordinate on the other hand.

(2) *Geometry and measurements*. The construction of 3D city models generally involves many more measurements than the 2D acquisition of the same real-world feature (e.g. height of the eaves of a roof, and position of a window on a wall).

(3) *Level of detail*. The models may be derived in multiple forms distinguished by levels of detail (LODs), different degrees of the abstraction from the real-world and the complexity of the spatio-semantic representation (Biljecki *et al.*, 2014c). The LOD concept usually does not cover the spatial accuracy, and when it does impose requirements, this is in practice frequently overlooked (Biljecki *et al.*, 2013). An arising research question is whether the LODs have an influence on the propagation of errors, and what is the magnitude.

(4) *Applications*. 3D city models are nowadays used for applications not possible with 2D data, such as the estimation of the energy demand of buildings (Strzalka *et al.*, 2011; Kaden and Kolbe, 2014), shadow estimation (Herbert and Chen, 2014), and visibility analyses (Bartie *et al.*, 2010). Further, they are used in applications that are considerably more complex than when used with 2D data, such as estimating noise pollution (Stoter *et al.*, 2008) and taxation (Boeters *et al.*, 2015).

The objective of this paper is to generalise the error propagation analysis to 3D GIS operations, and to investigate how the Monte Carlo method can be used to obtain insight into error propagation in one use case in 3D city modelling: the estimation of the solar irradiation on roofs of buildings, for the aim of assessing the suitability of the installation of photovoltaic (PV) modules for producing electric energy. This application is a widely used example of the use of 3D city models and it requires 3D GIS operations. For this study, we conducted an analysis for the city of Delft in the Netherlands with a software prototype that we have implemented ourselves, but the software is sufficiently generic to be applicable to other locations in the world.

We focus on the uncertainties of the geometry of the model, and investigate how positional accuracy influences the quality of a 3D spatial analysis. Positional accuracy is a prominent spatial data quality element, and a principal descriptor in the metadata of a geo-dataset. In most analyses the error in the position affects the outcome of a GIS operation.

The paper is organised as follows. Section 2 describes the related work and the research opportunities that we attempt to tackle. In Section 3 we detail the use case of the estimation of solar

irradiation of buildings with 3D city models, and explain the methodology and implementation of our software prototype. By giving a detailed description we aim for a better understanding of the process. Here we also bridge the literature gap because, despite its popularity, this 3D application has not been much described methodologically.

In Section 4 we describe the error propagation methodology and the implementation of an error engine that simulates acquisition errors to a procedural modelling engine. We run the extensive experiments on a procedurally generated dataset, and describe the results in Section 5. We finally present conclusions in Section 6.

2 Related work and research opportunities

The subject of error propagation is researched in several disciplines, such as physics (Taylor, 1997), medical imaging (Behrens *et al.*, 2003) and chemistry (MacLeod *et al.*, 2002), and it has a solid mathematical and experimental foundation that can be applied to other disciplines. It is related to GIS: geographical observations describe phenomena with spatial, temporal, and thematic components that are all acquired with uncertainty (Veregin, 2005). Besides measurement errors, uncertainty may be caused by processing, generalisation and several other factors (Fisher, 2005). Hence, understanding the propagation of errors in GIS is important. For instance, it is important to set expectations when obtaining and utilising datasets for a specific purpose. One may define a maximum acceptable uncertainty of the result of an operation, and by performing the analysis of the propagation of uncertainty within the operation may reversely determine the maximum allowed uncertainty in the input data. An example is the usage of 3D city models in estimating the visibility between two points in space. This technique is used by radio engineers and telecom companies to estimate the radio signal coverage (Wagen and Rizk, 2003), and for security purposes as in determining the optimal surveillance camera placement (Ying *et al.*, 2002; Yaagoubi *et al.*, 2015). While the first may be successfully accomplished with a rough and not overly accurate 3D city model, the latter relies on street-scale data where a comparatively small error may result in significant errors in the output.

The topic of error propagation has been researched and documented in numerous publications that go back several decades. Heuvelink *et al.* (1989) performed a quantitative analysis of gridded 2D data in a raster geographical information systems with two use cases, Arbia *et al.* (1998) modelled the error propagation of overlay operations in raster GIS, and Van Oort *et al.* (2005) researched the propagation of positional uncertainty of vertices in polygons to the computation of its area. Shi *et al.* (2005) researched the propagation of the error of the interpolation in digital elevation model (DEM), De Bruin *et al.* (2008) investigated the uncertainty of the input geographic data to planning costs in agriculture, and Shi *et al.* (2003) describes the propagation of buffer-related errors and completeness. Further, Heuvelink and Burrough (1993) investigated error propagation in cartographic modelling using Boolean logic and continuous classification. The documented analyses include the propagation of spatial errors and attribute errors, with the latter being more frequently represented. For instance, Veregin (1995) investigated the propagation of thematic errors.

To the best of our knowledge, there is no work published in the international scientific literature on uncertainty propagation in 3D spatial analysis. Shi (1998) presented a generic approach for modelling positional uncertainty in multi-dimensional objects, but did not address the propagation of uncertainty.

Propagated errors are defined as the discrepancies between performing identical operations on the true and on the observed, error-contaminated data layers. Error propagation modelling is the formal process of representing the transformations in data quality that occur through GIS operations on data layers (Arbia *et al.*, 1998). The error propagation problem can be formulated mathematically as follows (Heuvelink, 2005). Let $U(.)$ be the output of a GIS operation $g(.)$ on m inputs $A_i(.)$:

$$U(.) = g(A_1(.), \ldots, A_m(.)) \tag{1}$$

The operation $g(.)$ may represent virtually any GIS operation, such as stream network calculation from a DEM or electromagnetic field modelling from mobile phone base stations (Hengl *et al.*, 2010; Beekhuizen *et al.*, 2014). The objective of the error propagation analysis is to determine the error in the output $U(.)$, given the operation $g(.)$ and the errors in the inputs $A(.)$. The error or uncertainty is usually expressed with the variance of $U(.)$.

The Taylor series method, one of the two methods to assess the error propagation in GIS, requires the mathematical derivative of the operation $g(.)$. However, this method is not suited for complex operations since the derivative may not exist or be difficult to compute analytically. In contrast, the Monte Carlo method is made to work by running the assessment model repeatedly with random disturbances introduced into the uncertain inputs, where the degree of disturbance is in accordance with its uncertainty. When used in error propagation, it identifies the relationship between the input error distribution and that of the model outputs. Thus, it allows to determine whether the input error is amplified or is suppressed (Emmi and Horton, 1995). Following the previously introduced notation, the reasoning of the Monte Carlo method is to compute the result of $g(A_1, \ldots, A_m)$ repeatedly, with input values $A_i, i = 1, \ldots, m$ that are randomly sampled from their joint distribution (Heuvelink, 2005). The spread in the sample of m model outputs obtained in this way captures the uncertainty in the output.

Examples of the Monte Carlo method employed in the analysis of error propagation in GIS include an application in flood management (Qi *et al.*, 2013), a GIS-based assessment of seismic risk (Emmi and Horton, 1995), potential slope failures (Zhou *et al.*, 2003), natural resource analysis (Davis and Keller, 1997), interpolation of DEMs (Fan *et al.*, 2014), analysis of highway maintenance (Hong and Vonderohe, 2014), evaluation of the accuracy of agricultural land valuation using land use and soil information (Fisher, 1991), and the computation of building volumes (Biljecki *et al.*, 2014a).

3 Use case: annual solar irradiation with Solar3Dcity

The estimation of the solar irradiation at a location is one of the most prominent use cases in 3D GIS (see the recent literature review of Freitas *et al.* (2015)). The aim of this use case is to quantify "how sunny" a location is. This is done primarily for terrain (Kumar *et al.*, 1997; Zhang *et al.*, 2015) and for building roofs, mainly to assess the suitability and economic return of the installation of solar panels (Strzalka *et al.*, 2012; Li *et al.*, 2015). The latter application is gaining significant interest in the 3D city modelling research community and industry.

It is useful to introduce some terminology. Solar irradiance describes the *instantaneous* rate of energy that is being delivered to a surface (power per unit area), usually expressed in W/m^2. It varies depending on the location of the surface, time and date, atmospheric conditions, and other factors. The solar irradiation is the total amount of solar energy that has been collected on a surface area within a given time, i.e. solar irradiance *integrated* over time. It is also known as insolation, and it is typically expressed in kWh/m^2/year.

In case of determining the suitability of a photovoltaic installation on a surface, such as a building roof, the normalised solar irradiation value may be coupled with the area of the surface resulting in the solar irradiation of a surface in kWh/year. Contemporary solar panels are able to utilise only a fraction of this energy, but the exact amount also depends on additional factors, such as the ambient temperature. When estimating the amount of energy that can potentially be captured, we refer to the solar or photovoltaic potential (Wiginton *et al.*, 2010). Because solar potential depends on specific technical panel settings, and because the technology is continuously improving, in this research we focus on the perennial magnitude of the solar irradiation.

The use of GIS data and 3D city models in this use case is crucial. First, solar irradiation differs at different locations on Earth, i.e. due to different day lengths and the position of the Sun. Second, solar irradiance may significantly differ between building roofs in the same area, depending on the orientation of the roof: a more favourable angle of a surface to the sun means a better exposure and more solar energy. Two roof surfaces of the same size at the same location but of different orientations and inclinations (azimuth and tilt), may drastically differ in their solar potential (Yang and Lu, 2007; Santos *et al.*, 2014). This will also become evident from our experiments. Third, the larger the surface of a roof, the more solar energy is available, hence the information about the surface area of the roof is important as well.

3.1 General overview of the 3D use case

The solutions significantly vary from small to large-scale applications, each yielding a different spatial resolution of results. For instance, from a neighbourhood level with a value for each building (Wittmann *et al.*, 1997), to a national analysis for an average value for each municipality (Mainzer *et al.*, 2014) and global analyses as rasters of pixels of large size (Šúri *et al.*, 2005, 2007; Huld *et al.*, 2012). Perpendicularly, the complexity of the solutions vary from relatively

simple (clear-sky models) to complex solutions accounting for meteorological conditions, vegetation, and shadowing (Hofierka and Kaňuk, 2009; Tooke *et al.*, 2011; Nguyen and Pearce, 2012; Alam *et al.*, 2013; Liang *et al.*, 2015).

This paper deals with large-scale analysis (i.e. on buildings), which may be performed on different sets of data, e.g. voxels (Hofierka and Zlocha, 2012), LiDAR point clouds (Gooding *et al.*, 2015; Carneiro and Golay, 2009; Jochem *et al.*, 2009; Yu *et al.*, 2009), and the ones with building data, e.g. derived with a combination of LiDAR and GIS data (Jakubiec and Reinhart, 2013). While most of the work dealing with the solar potential of buildings is focused on rooftops, some extend the solar potential to vertical façades (e.g. Catita *et al.* (2014), Redweik *et al.* (2013), and Fath *et al.* (2015)).

In addition, supplementary information about buildings, such as the building type and number of inhabitants, may be used in order to relate the potential gain to the actual energy usage of the household (Baumanns and Löwner, 2009; Nouvel *et al.*, 2014). That is a reason why semantic 3D city models, such as CityGML data (Open Geospatial Consortium, 2012; Gröger and Plümer, 2012), are being increasingly used for this use case (Strzalka *et al.*, 2012; Ben Fekih Fradj and Löwner, 2012; Nouvel *et al.*, 2013). Performing the analysis with semantic 3D city models has further advantages over the aforementioned forms, e.g. the roof surfaces can be easily extracted for the analysis.

3.2 Methodology for the estimation of the solar irradiation with 3D city models

Solar radiation can be decomposed into three components (Šúri and Hofierka, 2004; Liang *et al.*, 2014), and these are analysed separately in the estimations. The radiation that is not reflected or scattered in the atmosphere and reaches the surface directly is known as *direct radiation*. The radiation scattered from atmospheric particles and clouds is called *diffuse radiation*. The part of the radiation that is reflected from the ground onto an inclined (roof) surface is denoted as *reflected radiation*. The three components of radiation together form the *global radiation*. Accounting for all three components is important, because in certain settings each may significantly differ (Gulin *et al.*, 2013b).

The estimation of the direct and reflected irradiation and their adjustment for the tilted and oriented surface are straightforward (Masters, 2013). The estimation of the diffuse solar irradiance is more complex, but there are several empirical models that can do this, and their comparison has been the subject of several research papers (David *et al.*, 2013; Demain *et al.*, 2013; Gulin *et al.*, 2013a).

That said, the solar irradiation I is estimated by integrating the solar irradiance E over a period of time: $I = \sum_{i=\text{start}}^{\text{end}} E_i \cdot \Delta t_i$, where Δt_i is the duration of the i^{th} time interval. Since the solar irradiance depends on the geographic location, from a GIS point of view, the solar irradiation I of a surface at a location $[\varphi, \lambda, h]$, with tilt τ, azimuth α, and area A may be seen as a function:

$$I = f([\varphi, \lambda, h], \tau, \alpha, A, [w]) \tag{2}$$

where φ, λ, and h indicate the latitude, longitude, and elevation of the surface, and $[w]$ denotes a series of other components such as meteorological conditions. Since the model f is complex, the propagation of errors can best be solved numerically with the Monte Carlo method, involving a large number of building models and disturbances of simulated input errors.

Considering the large number of simulations, in our work we do not take into account shading effects since these entail computationally expensive algorithms.

3.3 Design and implementation of Solar3Dcity

Because there is a lack of open-source software package for the use case, we designed and implemented our own software prototype "Solar3Dcity". The software supports data stored according to the OGC standard CityGML, and can handle large datasets, which is a requirement for a Monte Carlo simulation. Another motivation for building our own software is that it enables creating a custom format for the exchange of the results in the way that is suitable for our workflow.

Figure 1 shows the general workflow of the software which consists of deriving four geographic parameters for each building, these are essential for the solar potential analysis: area of the roof, tilt, azimuth, and the geographic location of the surface. The latter value is important in order to compute the solar ephemeris for a location on Earth and to retrieve the historical irradiance data, but note that it will not vary between buildings on a local basis, as the values do not change within the spatial extent of a typical city. Likewise, it is important to emphasise that this value is not affected by positional errors, unless they are caused by gross errors, for instance, wrong coordinate reference system, which is beyond the scope of this paper.

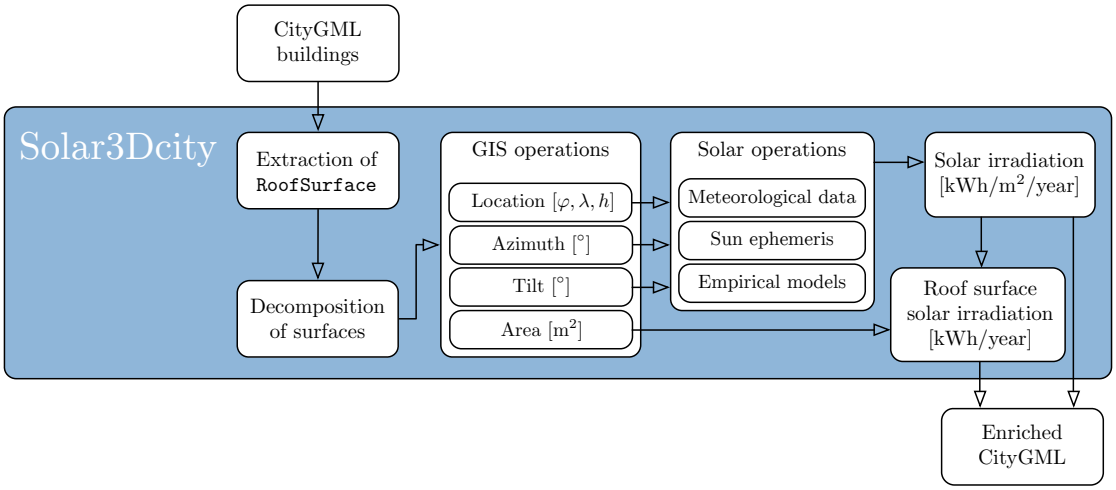

Figure 1: Software architecture of Solar3Dcity. The implementation reads semantic 3D city models in the CityGML format, extracts the surfaces that represent the roof, and enriches them with the value of the annual solar irradiation and with the total value for all roof surfaces of a building.

Because a roof can consist of more than one planar surface, the annual solar irradiation is calculated separately for each surface, and their values are summed up to obtain a single value of the total solar irradiation in kWh/year for a building under the assumption that all roof surfaces are suitable for the installation of the photovoltaic panels. However, it is not economically feasible to install solar panels in all cases (Lukač *et al.*, 2013; Eicker *et al.*, 2014), e.g. on a small roof area that does not get much sunlight, hence we define the filtered total building solar irradiation, which is the total irradiation excluding roof surfaces that are smaller than 2 m^2 and have a solar irradiation smaller than 850 kWh/m^2/year. Note that introducing this filter is also interesting in the analysis of the propagation of errors, because the determination of whether a surface passes this filter is prone to input errors, and it can potentially result in Type I (false positives) and Type II (false negatives) errors (i.e. rejecting a surface that is in reality suitable, and vice-versa).

Before the computations, each surface is geometrically validated (e.g. non-planar surfaces and self-intersecting boundaries), ruling out invalid cases occurring in real-world data and making this implementation robust. The solar ephemeris are from PyEphem/XEphem* (Meeus, 1998; Bretagnon and Francou, 1988), which have been proven suitable for solar radiation studies (Reda and Andreas, 2004). The computations use the empirical anisotropic model developed by Perez *et al.* (1990), which was implemented in the Solpy library†. The historical solar irradiance data, which are important to reflect the actual climatic conditions and to approximate a typical meteorological year (Kalogirou, 2003), are taken from the nearest meteorological station (in our case from the IWEC dataset—International Weather For Energy Calculations; Thevenard and Brunger (2002)). The annual global solar irradiation is then calculated for each roof by integrating the hourly irradiance values of the entire year (similar to the approach of Mardaljevic and Rylatt (2003)).

To remove redundancy and to speed up computations, we precomputed the normalised function $ir = f([\varphi, \lambda, h], \tau, \alpha)$ for the location of the study area (i.e. the city of Delft in this study). Once the orientation of a surface is estimated from the 3D city model, the software samples the irradiation value from the function, rather than doing the computations all over again. Figure 2 shows the values of such function, i.e. the solar irradiation in kWh/m^2/year for every azimuth/tilt combination. This function, also known as *tilt-orientation-factors* (TOF), is also a product itself since it helps finding the optimal tilt and orientation for a location, which is the main aim of several location-based studies (Šúri *et al.*, 2005; Christensen and Barker, 2001; Rowlands *et al.*, 2011). The last component, i.e. the area of the surface, is thence multiplied with this normalised irradiation value to obtain the irradiation of the roof surface.

After the irradiation is computed, the value of the estimated annual solar irradiation per building and its roof surfaces are stored in the CityGML file. An example of the visualisation of such enriched CityGML file is shown in Figure 3.

*`https://pypi.python.org/pypi/pyephem/` and `http://www.clearskyinstitute.com/xephem/`
†`http://github.com/nrcharles/solpy`

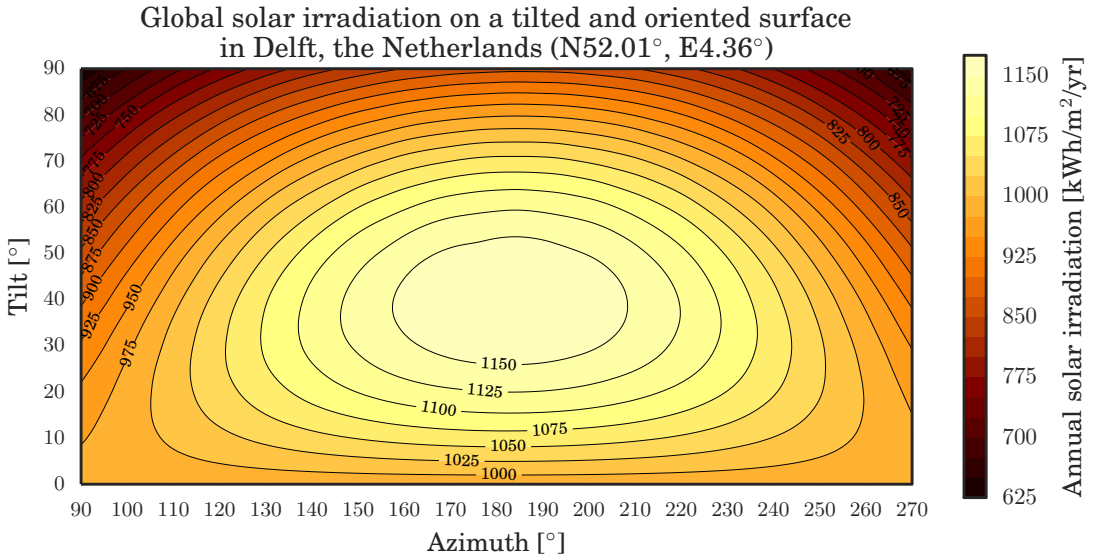

Figure 2: The annual global solar irradiation for Delft as a function of tilt and azimuth, as estimated by Solar3Dcity. The centre of the plot is facing south, and it is bounded by west and east facing surfaces, meaning that this is only half of the complete function. Values for surfaces facing north are further decreasing. The plot shows significant variation of the solar irradiation between differently tilted and oriented surfaces, showing the importance of 3D city models and GIS operations in this application.

4 Methodology and implementation

4.1 Overview

The uncertainty propagation method involves four main steps (Figure 4):

1. Generate a set of buildings in a parametric and spatio-semantic form (3D city models) with procedural modelling (Biljecki *et al.*, 2015a). We use procedural models mainly because it is easier to disturb these with simulated acquisition errors, because they provide a free and unlimited source of diverse settings, and because the ground truth is known. Synthetic data have been used for similar purposes, for instance analysing bathymetric models (Li *et al.*, 2000), uncertainty in land cover maps (Burnicki *et al.*, 2007), and assessing classification performance (Gosselin and Cord, 2006).

2. Perturb the simulated *base* dataset generated in the first step repeatedly with random disturbances sampled from the probability distribution representing the geometrical errors. For this we implemented an error engine that builds on top of the procedural modelling engine by *injecting* errors in the process.

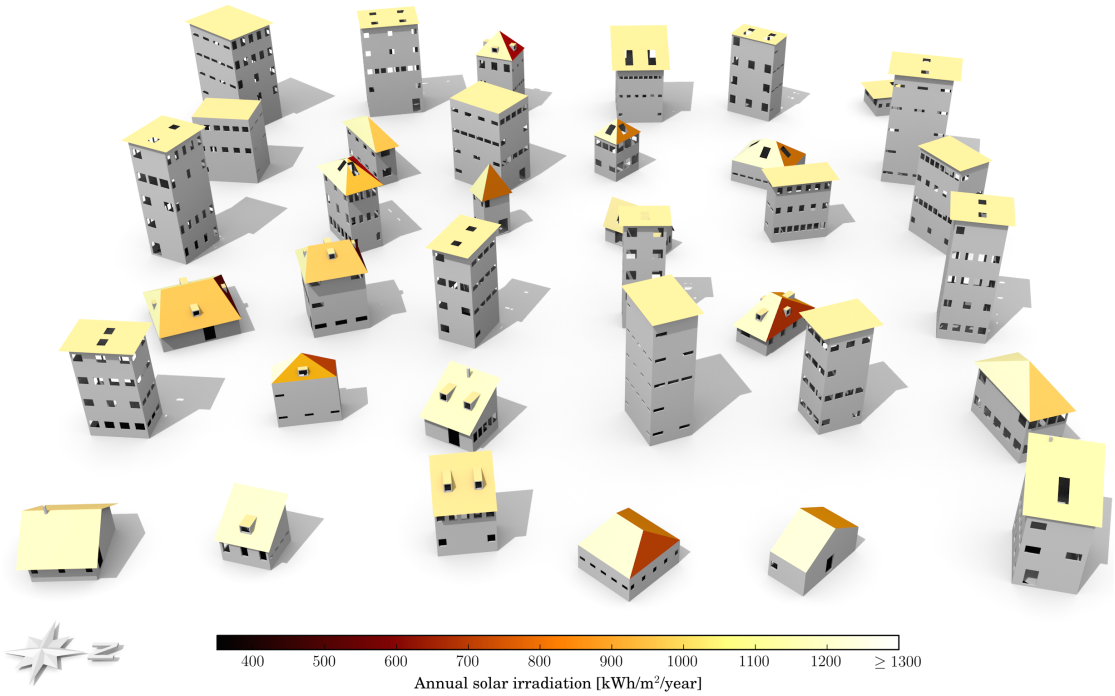

Figure 3: The roofs in this example CityGML dataset are coloured based on how much solar energy they receive in one year per square metre (normalised annual insolation). The orientation of the north is shown in the bottom left part of the figure. To put these values in perspective for the experiments: a rooftop of a building with an optimally inclined shed roof of an area of 100 m^2 and without roof windows receives around 117 MWh of solar energy per year.

3. Analyse both the ground truth and erroneous models with Solar3Dcity to estimate the solar irradiation of roofs.

4. Compute the errors in the solar estimations, and calculate common uncertainty measures such as the Mean Error (ME) and Root Mean Square Error (RMSE).

4.2 Considered levels of detail

3D city models may be derived in multiple LODs, i.e. degrees of spatio-semantic complexity that reflect the intended use case and the spatial resolution of the models (Biljecki *et al.*, 2014c). Because the LODs represent different degrees of abstraction of reality, it is interesting to investigate how acquisition errors propagate depending on the LOD.

The most common LOD categorisation is the one of the CityGML standard (Open Geospatial Consortium, 2012; Gröger and Plümer, 2012; Kolbe, 2009), which defines five LODs: LOD0–4.

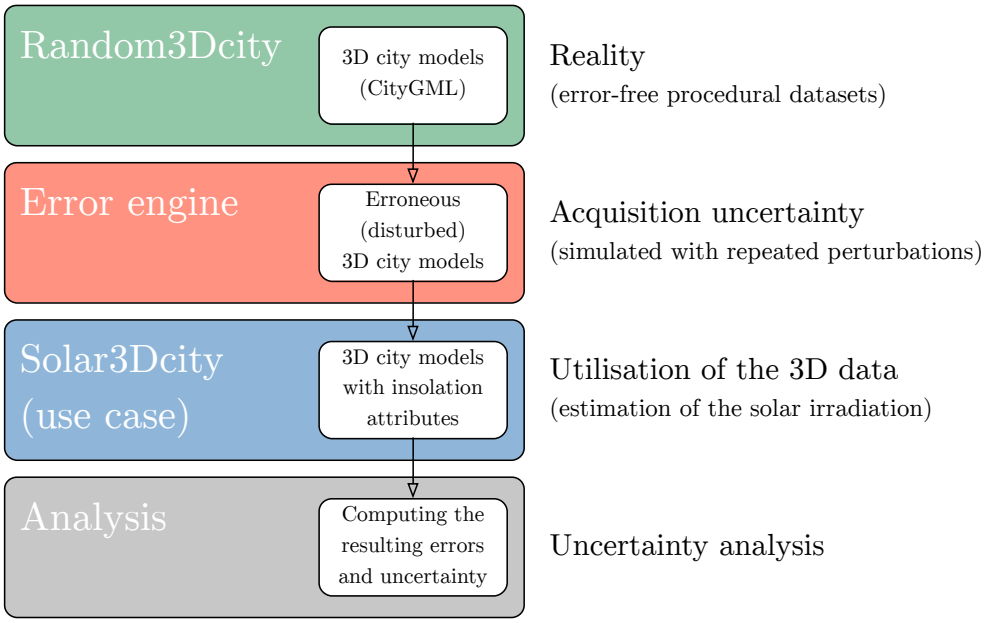

Figure 4: Workflow of the uncertainty propagation analysis. Each part is a separate software module, and data flows from one to the other. The third module is detailed in Figure 1.

Because LOD0 is a 2.5D representation, and LOD4 is a model that contains the building interior, we restrict our analysis to the three intermediate LODs.

LOD1 is a block model with flat *roofs* that is usually derived as an extrusion from 2D footprints with point cloud data (Ledoux and Meijers, 2011; Arroyo Ohori *et al.*, 2015b). This is a coarse model in which regardless of the roof shape, the top surfaces have the same orientation and tilt (they are flat). Hence their value in this use case is questionable. While they provide a good approximation of a building with a flat roof, in reality, when solar panels are installed on flat roofs they are not laid flat (Bayod-Rújula *et al.*, 2011), as they are optimally oriented according to models similar to the one shown in Figure 2 (Eicker *et al.*, 2015). This is a different practice from that used in case of non-flat roofs, where the solar panels are laid on the roof, essentially retaining the same orientation as the underlying roof surface. Nevertheless, in our analysis we include LOD1 models, to investigate whether the uncertainty propagation differs between different LODs.

LOD2 is a model with simple roof shapes, and is most commonly used in solar potential analyses worldwide. Conceptually, LOD2 models provide the exact tilt and azimuth of the roof, and they are relatively straightforward to acquire (e.g. see Haala and Kada (2010) and Musialski *et al.* (2013)). However, LOD2 models usually do not include dormers and roof windows, hence they tend to have a systematically larger roof area than in reality. Further, the LOD2 standard is flexible, meaning that LOD2 models may include dormers and similarly sized roof superstructures. For this reason we follow the specification of Biljecki *et al.* (2015a) who define two variants of LOD2: LOD2.1 which has "clean" roof structures, and LOD2.2, which includes dormers and similar roof superstructures.

LODs 1 and 2 may come in two geometric references for the footprint: with the walls at their actual position and as projections from the roof edge (Biljecki *et al.*, 2014b; INSPIRE Thematic Working Group Buildings, 2013). The latter variant accounts for roof overhangs bringing the roof to its more accurate representation, hence this variant is used here.

LOD3 is a detailed architectural model which contains dormers, roof windows and other smaller roof features (see the models in Figure 3). For LOD3 models, Monte Carlo simulations have not been performed with values of σ greater than 0.3 m, because acquisition techniques should be more accurate in the case of LOD3 than in the case of LODs 1 and 2.

4.3 Procedural models and their perturbation

Procedural modelling is a process of constructing 3D city models from scratch or based on an existing GIS dataset by using a set of rules (Goetz, 2013; Tsiliakou *et al.*, 2014). There have been several initiatives to develop procedural engines for modelling urban features, such as buildings (Wonka *et al.*, 2003; Müller *et al.*, 2006; Kelly and Wonka, 2011; Besuievsky and Patow, 2013), roads (Beneš *et al.*, 2014), and land parcels (Vanegas *et al.*, 2012).

While they have many potentials as it will become evident from our research, procedural models have not been used before in uncertainty propagation. For this purpose we use Random3Dcity, an open-source CityGML procedural modelling engine developed by Biljecki *et al.* (2015a). The engine first generates a real-world feature (e.g. a building) F_i by deriving a set of n parameters p_i that unambiguously define it:

$$F_i = \{p_i^1, p_i^2, \ldots p_i^n\} \tag{3}$$

The generation of buildings is done according to a customisable shape grammar and set of rules that generate realistic buildings. We adapt the procedures to generate buildings that are representative for our study area, where smaller residential buildings with sloped roofs dominate.

These parameters correspond to those used in photogrammetry (e.g. *cf.* Brenner (2005); Zhang *et al.* (2014)), such as the width of a building, size of the ridges, eaves, and roof height. They are stored in a parametric form (e.g. the height from the lowest point to the eaves of the building F_i: $p_i^h = 6.54$ m), from which the second part of the engine then generates a 3D city model in multiple LODs stored in CityGML.

However, in reality, we do not know the true parameter values because these are subject to observation error. Hence, we represent the true parameter value by a random variable that is modelled as the sum of the parameter estimate and a zero-mean, normally distributed stochastic error ϵ, resulting in the uncertain parameter $\widetilde{p^j} = p^j + \epsilon^j$.

Therefore, between the first (parametric) and the second (3D city model realisation) step we insert a stochastic engine that *degrades* the parameters by sampling values from a normal probability distribution function with standard deviation σ:

$$\widetilde{p}_i^j = \mathcal{N}(p_i^j, \sigma^2) \tag{4}$$

Simulating acquisition errors with an uncertainty engine is in line with other error propagation analysis methods (e.g. see Brown and Heuvelink (2007); Heuvelink *et al.* (2007); Ben-Haim *et al.* (2014)). In the engine we use the normal distribution because it is commonly used in geomatics (Goodchild, 1991; Caspary and Scheuring, 1993), and because it has a theoretical underpinning through the Central Limit Theorem from statistics.

The above results in an erroneous version of the building $\widetilde{F}_i = \{\widetilde{p}_i^1, \widetilde{p}_i^2, \ldots \widetilde{p}_i^n\}$, e.g. for the aforementioned height example we might get $\widetilde{p}_i^h = 6.71$ m when using $\sigma = 0.2$ m. The engine can generate an infinity of erroneous versions of the building by repeating the perturbation method, each time sampling a new from the probability distribution of the parameter error.

Disturbing the parameters rather than the coordinates of the geometry of the generated 3D city model has several advantages: it is more straightforward, it diminishes the chances of creating degenerate geometries (e.g. non-planar surfaces and invalid solids), and it conforms to the real-world practices of acquisition of 3D city models. Most software packages nowadays facilitate modelling of buildings by measuring the distances of buildings' lengths at right angles (Loch-Dehbi and Plümer, 2011), especially in automatic workflows (Fischer *et al.*, 1998). Further, as the noise is added to the parameters, which represent the lengths of the edges, the right angles in the geometry are then preserved. Finally, there is also a data specification justification. Consider that a project requires the acquisition of buildings as LOD1 block models with a flat top surface, which regardless of the acquisition errors are then always block models. If in our approach the coordinates of the geometry were disturbed, the noise in the geometry would result in non-flat top surfaces breaking the specification, which is different from the reality.

4.4 Varying uncertainty in 2D/3D and multiple accuracy classes

In 3D GIS, the accuracy $\sigma_{x,y}$ of lateral coordinates (X, Y) and the accuracy σ_z of vertical coordinates (Z) in the geometry are often different. This is due to two reasons. First, 3D city models are often constructed by combining multiple acquisition techniques. For instance, LOD1 block models are derived by extrusion with the combination of cadastral footprints, while heights are obtained from aerial laser scanners (LiDAR) (Ledoux and Meijers, 2011). This is often the case for LOD2 as well. Second, within the same acquisition technique, the accuracy levels may vary. For instance, the specification of the LiDAR system ALS70-CM from Leica (2008) states "The system produces data after post processing with a lateral placement accuracy of 5–38 cm and vertical placement accuracy of 7–16 cm (one standard deviation) [...]". Hence, varying uncertainty levels are one of the important characteristics of 3D modelling to consider for uncertainty propagation.

Therefore, for $\sigma_{x,y}$ and σ_z we define a series of 11 accuracy classes (ranging from 0.0 to 1.0 m with 0.1 m increments), and permute them resulting in 121 combinations, e.g. $\sigma_{x,y}$ = 0.3 m / σ_z = 0.6 m. We choose these ranges to describe the current capabilities of acquisition techniques, and these

are in accordance to the ranges determined by research efforts that investigate the accuracy of 3D city models (Kaartinen *et al.*, 2005; Gruber *et al.*, 2008; Oude Elberink and Vosselman, 2011; Rottensteiner *et al.*, 2014; Harwin and Lucieer, 2012). The *0th* accuracy class ($\sigma_{x,y} = \sigma_z = 0$) has been considered as well in order to ensure that there are no errors in our implementation of simulating uncertainty.

Monte Carlo simulation requires that the model is run repeatedly with different perturbations (*cf.* Emmi and Horton (1995)), commonly in a large number m (in our experiments we used $m = 2000$). Hence, in the workflow each building in each perturbation d is disturbed in 121 different ways, resulting in an erroneous building $\widetilde{F}_i^{j,k}, j = 1, \ldots, 121; k = 1, \ldots, m$.

Finally, after the perturbations of the parameters, all simulated 3D city models are input in the solar irradiation analysis (see Figure 5 for an example). Variability between solar irradiation resulting from the perturbation characterises how uncertainty about a building's geometry propagates to its solar irradiation.

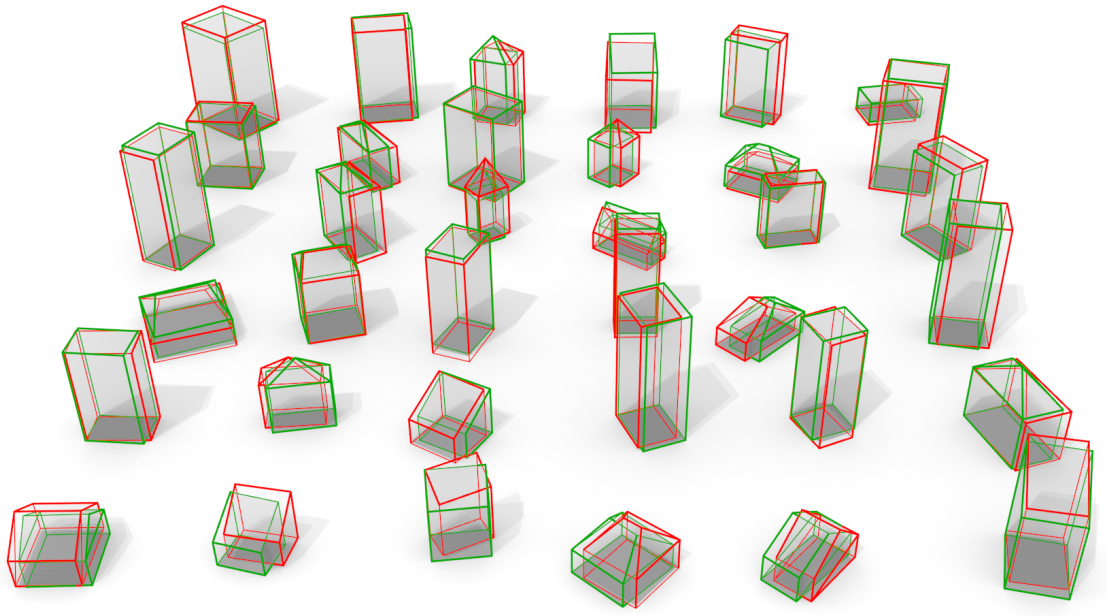

Figure 5: Composite of the geometry of two LOD2.1 models of the buildings shown in Figure 3: the green model is the ground truth, while the red model has been disturbed with errors using $\sigma_{x,y} = \sigma_z = 0.4$ m. Note that this is only one of the considered 121 accuracy classes, showing the outcome of only one of the 2000 iterations in one LOD, meaning that in our experiments there are 758 000 datasets in total (242k for each of LOD1, LOD2.1, LOD2.2, and 32k for LOD3 due to the reduced accuracy classes).

4.5 Errors and measures of uncertainty

We computed the following error measures for each accuracy class and each LOD:

- RMSE of the estimated tilt, azimuth, and area of the roof surfaces.
- RMSE of the annual irradiation in kWh/m^2/year of roof surfaces.
- RMSE of the building rooftop annual irradiation in kWh/year.
- RMSE of the filtered building rooftop annual irradiation in kWh/year, i.e. those surfaces that fulfil the minimum thresholds of the normalised annual irradiation and area (Section 3.3).
- The share of false positives and false negatives in determining the feasibility of installing a solar panel (in %). This analysis is Boolean (a surface is feasible or not), hence we are computing the share of errors in the total number of estimations.

To put these values in perspective, for each RMSE, also the relative RMSE in percentage has been computed. As ground truth we take the undisturbed model ($\sigma = 0$) of the building in that LOD. Further, for all cases the distribution of errors is examined.

5 Experiments, results, and discussion

We conducted the experiments with 100 procedurally generated buildings located in Delft in four LODs in 121 accuracy classes in repeated perturbations of 2000 Monte Carlo iterations. We chose this number of iterations because it produced sufficiently stable results without requiring too much computing resources.

This results in about 75.8 million 3D building models that have to be analysed. The performance of disturbing the models, generating the CityGML files and computing their annual solar irradiation is on average 80 models per second, which resulted in about two weeks of computation (the speed of solely computation of the solar estimations amounts to 1000 buildings per second thanks to the precomputed function; see Figure 2).

Due to the large number of results, we focus on the most important results only. Figure 6 shows the propagation of positional error to the error in the estimation of the total building irradiation and to the filtered (feasible) value. Because of limited space we show this for 11 classes where $\sigma_{x,y} = \sigma_z$. The plot shows that the relation between the uncertainty in the input and uncertainty in the output is linear, and that the results for each LOD are practically equal, with the exception of LOD1. The smaller error of the LOD1 can be explained by the absence of errors in the tilt and azimuth (the top surface is always flat, as imposed by the model specification), hence only the uncertainty in the area has an influence.

Because the uncertainty propagation in LOD2.1, LOD2.2 and LOD3 is equivalent, from here we will present the results of one of these LODs. Figure 7 shows the propagation of positional

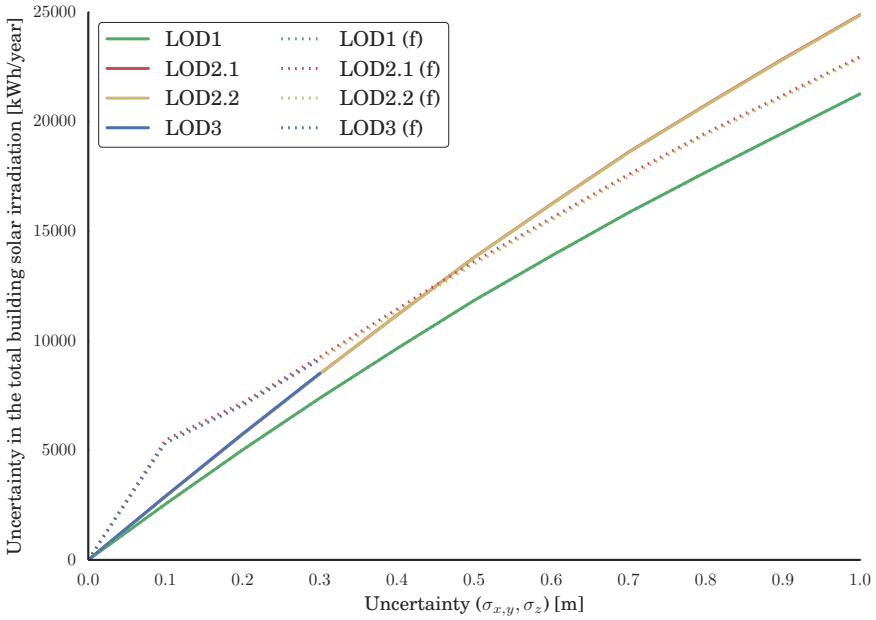

Figure 6: Propagation of positional error in case $\sigma_{x,y} = \sigma_z$ to the total building irradiation (sum of the insolation of all roof surfaces), and to the filtered value, indicated by (f), where only feasible surfaces are taken into account. Note that the values for LOD2.1, LOD2.2, and LOD3 are equal.

uncertainty to the uncertainty of the three components required for computing the solar irradiation: azimuth, tilt, and area. The figure also shows the RMSE of the normalised irradiation [kWh/m^2/year] for each uncertainty class. Note that in computing the value of the normalised solar irradiation, the area has not been used (which was used for the total building irradiation [kWh/year], shown later).

Since the values of the uncertainty in the solar irradiation may be of interest to practitioners, we provide them in Table 1. The plots show a different degree of the influence of the planar and vertical positional uncertainty. For instance, the estimation of the orientation of the roof is not affected by the vertical uncertainty. Obviously, the exact results depend on the analysed setting (i.e. location, empirical model, etc.), but we believe that the general conclusions presented here are consistent for most, if not all scenarios.

Figure 8 and Table 2 provide the uncertainty in the estimation of the total solar irradiation of roof surfaces of buildings for all accuracy classes. The results show that at smaller planar uncertainties, the vertical positional uncertainty influences the total irradiation uncertainty, while for greater planar uncertainties its influence is negligible.

Figure 9 shows the Type I and Type II errors for the estimation of the feasibility of installing a solar panel. Finally, Figure 10 shows the distribution of errors for various settings (LODs and uncertainties). It appears that regardless of the setting, the errors are distributed according to

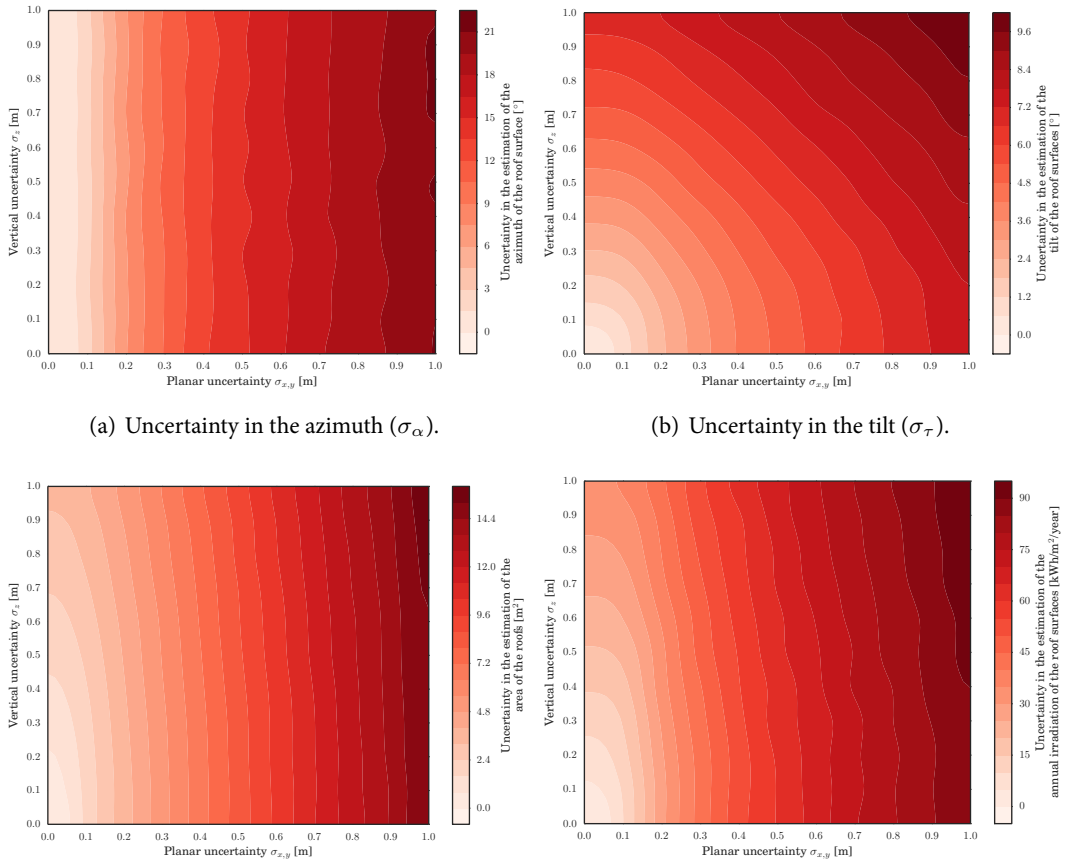

(a) Uncertainty in the azimuth (σ_α).

(b) Uncertainty in the tilt (σ_τ).

(c) Uncertainty in the area (σ_A).

(d) Uncertainty in the normalised irradiation (σ_{ir}).

Figure 7: Results of the error propagation experiments on the uncertainty of the three components of the estimation of the irradiation (azimuth, tilt, area), and the normalised irradiation.

Table 1: Standard deviation of the estimation of the normalised irradiation of roof surfaces of buildings [kWh/m^2/year], estimated for the 121 accuracy classes. The bracketed values indicate the relative RMSE in percents.

σ_z [m]	$\sigma_{x,y}$ [m] 0.0	0.1	0.2	0.3	0.4	0.5	0.6	0.7	0.8	0.9	1.0
0.0	0 (0)	10 (1)	28 (4)	42 (6)	53 (8)	60 (9)	67 (10)	74 (11)	80 (12)	84 (13)	90 (13)
0.1	4 (1)	11 (1)	28 (4)	42 (6)	53 (8)	60 (9)	67 (10)	73 (11)	80 (12)	85 (13)	90 (13)
0.2	8 (1)	13 (2)	29 (4)	42 (6)	52 (8)	61 (9)	68 (10)	74 (11)	79 (12)	84 (13)	89 (13)
0.3	12 (2)	15 (2)	31 (5)	43 (7)	54 (8)	62 (9)	68 (10)	74 (11)	80 (12)	85 (13)	90 (14)
0.4	16 (2)	18 (3)	33 (5)	45 (7)	55 (8)	62 (9)	69 (10)	76 (11)	80 (12)	87 (13)	90 (14)
0.5	19 (3)	22 (3)	34 (5)	47 (7)	55 (8)	64 (10)	69 (11)	75 (11)	82 (12)	87 (13)	91 (14)
0.6	23 (3)	25 (4)	36 (5)	47 (7)	57 (9)	64 (10)	70 (11)	77 (12)	82 (12)	87 (13)	91 (14)
0.7	26 (4)	28 (4)	39 (6)	49 (7)	58 (9)	66 (10)	72 (11)	77 (12)	83 (13)	88 (13)	93 (14)
0.8	29 (4)	31 (5)	40 (6)	51 (8)	59 (9)	66 (10)	73 (11)	79 (12)	84 (13)	88 (13)	93 (14)
0.9	32 (5)	33 (5)	42 (6)	53 (8)	60 (9)	67 (10)	74 (11)	79 (12)	84 (13)	89 (14)	94 (14)
1.0	34 (5)	36 (5)	44 (7)	54 (8)	62 (9)	68 (10)	74 (11)	80 (12)	85 (13)	90 (14)	94 (14)

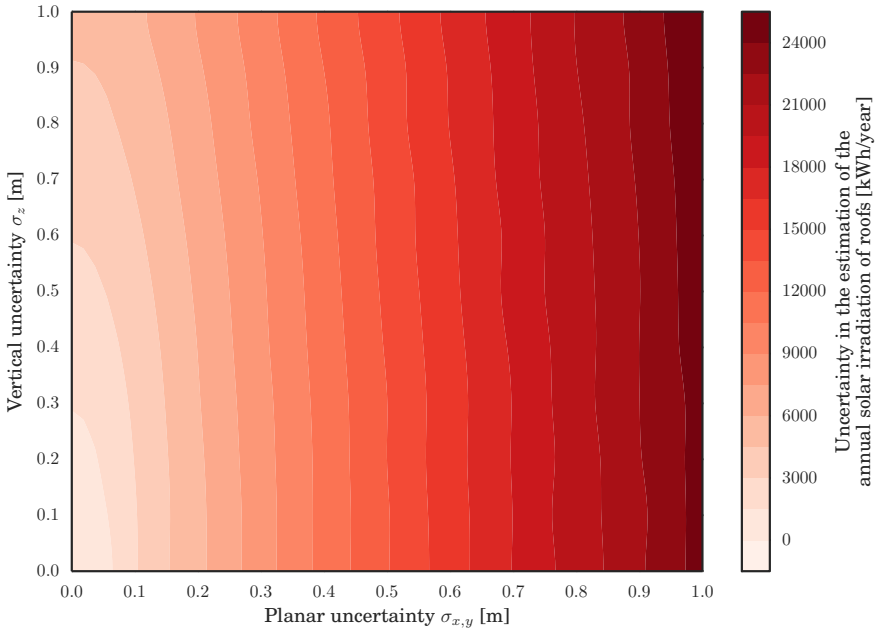

Figure 8: Uncertainty in the estimation of the total irradiation of a building (σ_I).

Table 2: Standard deviation of the estimation of the total global solar irradiation of roof surfaces of buildings [MWh/year], estimated for 121 accuracy classes. The bracketed values indicate the relative RMSE in percents.

σ_z [m]	$\sigma_{x,y}$ [m] 0.0	0.1	0.2	0.3	0.4	0.5	0.6	0.7	0.8	0.9	1.0
0.0	0.0 (0)	2.8 (5)	5.6 (10)	8.3 (15)	11.0 (21)	13.4 (25)	15.8 (30)	18.1 (34)	20.2 (37)	22.3 (41)	24.2 (44)
0.1	0.5 (1)	2.9 (5)	5.6 (11)	8.3 (16)	10.9 (20)	13.4 (25)	15.8 (30)	18.0 (34)	20.3 (38)	22.2 (41)	24.2 (44)
0.2	1.0 (2)	3.1 (6)	5.7 (11)	8.4 (16)	11.0 (21)	13.5 (25)	15.9 (30)	18.1 (34)	20.2 (38)	22.4 (41)	24.2 (44)
0.3	1.6 (3)	3.3 (6)	5.9 (11)	8.5 (16)	11.0 (21)	13.5 (25)	15.9 (30)	18.1 (34)	20.4 (38)	22.5 (41)	24.2 (44)
0.4	2.1 (3)	3.5 (6)	6.0 (11)	8.7 (16)	11.2 (21)	13.6 (25)	16.0 (30)	18.2 (34)	20.4 (38)	22.5 (41)	24.4 (44)
0.5	2.6 (4)	3.9 (7)	6.2 (11)	8.8 (16)	11.3 (21)	13.8 (26)	16.1 (30)	18.4 (34)	20.5 (38)	22.5 (41)	24.4 (45)
0.6	3.1 (5)	4.2 (7)	6.5 (12)	8.9 (16)	11.5 (21)	13.9 (26)	16.2 (30)	18.4 (34)	20.5 (38)	22.5 (41)	24.5 (44)
0.7	3.5 (6)	4.6 (8)	6.7 (12)	9.1 (17)	11.6 (22)	14.0 (26)	16.3 (30)	18.6 (34)	20.6 (38)	22.7 (41)	24.5 (45)
0.8	4.0 (6)	5.0 (8)	7.0 (12)	9.4 (17)	11.8 (22)	14.2 (26)	16.6 (31)	18.7 (34)	20.8 (38)	22.8 (42)	24.6 (45)
0.9	4.4 (7)	5.3 (9)	7.3 (13)	9.6 (17)	12.0 (22)	14.3 (27)	16.6 (31)	18.8 (35)	21.0 (38)	22.9 (42)	24.8 (45)
1.0	4.9 (8)	5.7 (10)	7.6 (13)	9.9 (18)	12.3 (23)	14.5 (27)	16.8 (31)	18.9 (35)	21.1 (39)	23.1 (42)	24.9 (45)

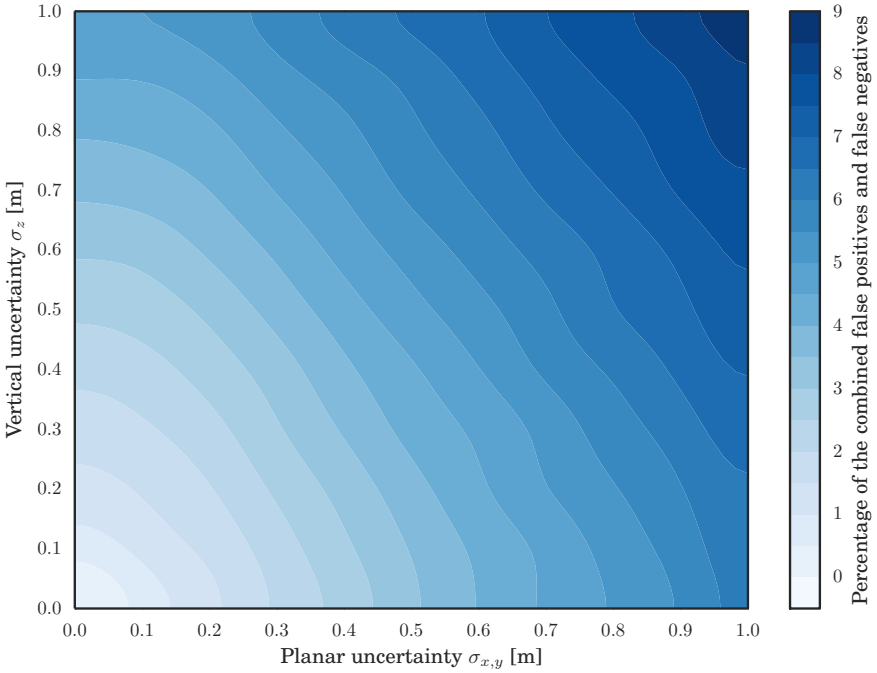

Figure 9: The summed false positives (Type I errors) and false negatives (Type II errors) in the determination of the feasibility of a photovoltaic installation on a roof surface.

a symmetric probability density function. However, none of the distributions is normally distributed. This was tested with a normality test of D'Agostino (1971) that combines skew and kurtosis to produce an omnibus test of normality, and by attempting to fit a function (also shown in the Figure 10).

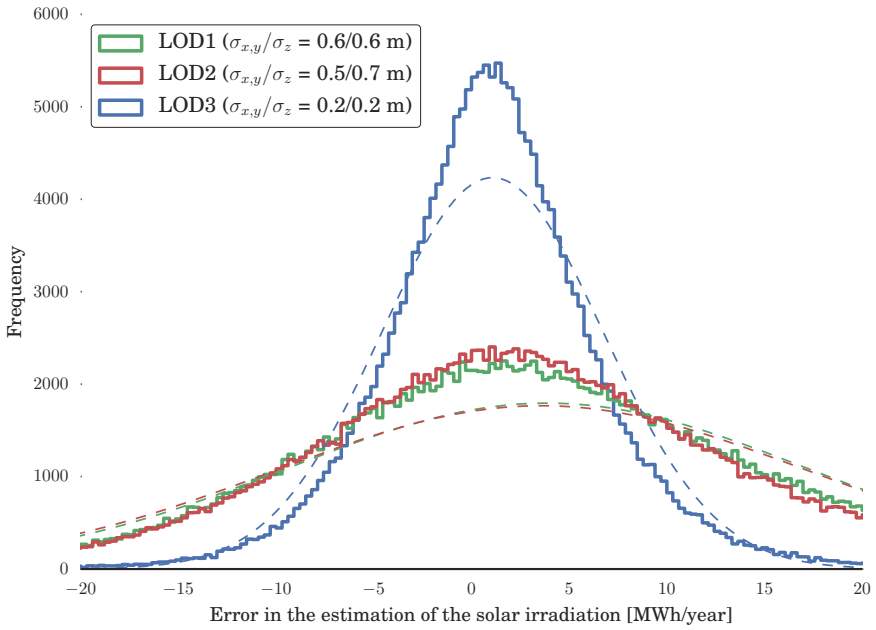

Figure 10: Distribution of errors in the estimation of the annual solar irradiation for a building, for three configurations (LOD and uncertainty class $\sigma_{x,y}/\sigma_z$), and the attempted fit of the normal distribution for each (dashed in the corresponding colour).

From the results, the following conclusions can be drawn:

- The propagation of errors is similar for LOD2 and LOD3. For LOD1 it is smaller, but the usability of these results is doubtful because LOD1 imposes flat roofs and involves a large model error which is not taken into account in the error propagation analysis.
- LOD3 models are equally prone to errors as LOD2 models. Hence, it does not make sense to acquire a high LOD if the acquisition method is not very accurate. For solar irradiation calculations, in most cases there is no substantial added value in replacing LOD2 models with LOD3 models.
- The planar and vertical accuracy have a different influence on the output uncertainty, hence it is important to consider these separately.
- The mean error deviates from zero in most cases which suggests a systematic error in solar irradiation. This can be explained from the non-linear relationship between uncertain parameters and solar irradiation.

- The errors in the estimation of the feasibility of installing a solar panel on a roof surface may reach approximately 10% at σ = 1.0 m (i.e. 10% of roof surfaces are deemed feasible for the installation of solar panels while in reality they are not, and vice-versa), which indicates that in many occasions 3D models acquired in this and coarser range of uncertainty, may not be suitable for this use case.
- Relatively, the propagation of error in the estimation of the normalised solar irradiation is smaller than in the estimation of the total building rooftop solar irradiation (normalised irradiation multiplied with the roof surface area), because the calculation of area is more sensitive to the uncertainty in the input data.

6 Conclusions and future work

In this paper we have performed a 3D GIS error propagation analysis involving 3D city models and their application for estimating the solar irradiation of roofs. The analysis involved the use of procedurally generated 3D city models, and it took into account multiple LODs in multiple accuracy classes with varying dimensional accuracy, all of which are novelties in the research field. The uncertainty propagation analysis enabled us to calculate the uncertainty in the estimated solar irradiation based on the specified uncertainty in the input data, and it gave us detailed insights.

For example, the uncertainty analysis showed that on average a 0.4/0.3 m positional error causes an uncertainty of about 8700 kWh/year in the estimation of the total annual insolation of the roof of a building, which is approximately a relative deviation of 16%. Another important insight is that the GIS components required for estimating the solar irradiation of a roof surface of a building (azimuth, tilt, area), show a different sensitivity to the input uncertainty, and that the planar and vertical uncertainty have a different influence on the estimations.

The obtained results are of importance to practitioners that rely on 3D city models for the estimation of the solar irradiation of buildings. They need this type of information to be able to decide whether installing solar panels is economically attractive. The uncertainty quantification extends such analysis by allowing us to take the risk of making wrong decisions into account. These observations may also be important to practitioners dealing with related applications of estimating the solar irradiation on a building, such as in urban planning (Yasumoto *et al.*, 2012; Vermeulen *et al.*, 2015), for research into the thermal comfort of buildings (Chwieduk, 2009), indoor illuminance (Saran *et al.*, 2015), crisis management (Aarsen *et al.*, 2015), and in the valuation of real estate (Helbich *et al.*, 2013).

We used procedurally generated (synthetic) 3D city models, which proved suitable for this purpose. An important advantage of using procedural models is that these present an unlimited source of diverse data, especially when it comes to obtaining data in multiple LODs, which are rare in practice (Biljecki *et al.*, 2015b). Our instance takes advantage of the availability of LOD3, since in the computation of the area, it accounts for roof windows, roof overhangs and dormers and chimneys, which decrease and increase, respectively, the area and configuration of the roof that is usable for photovoltaic panel installations. Having the information about roof windows is

important, but it is frequently not possible due to lack of highly-detailed data and this information is in practice supplemented manually with surveys on site (Nouvel *et al.*, 2013).

While we have focused on this use case, much of the developed work is applicable to other 3D use cases, such as noise estimation, energy demand estimation, and estimation of shadow cast by buildings.

For estimating the solar irradiation of roofs, we have implemented a new software prototype "Solar3Dcity". To make our method generally applicable, we enabled Solar3Dcity to be applicable to any location on Earth. Further, we have released this tool open-source for free public use.

For future work we plan to extend the work by investigating the propagation of uncertainty on continuous LODs (Arroyo Ohori *et al.*, 2015a), to take into account shadows (Nguyen and Pearce, 2012), and to investigate how the errors in estimated solar irradiation will propagate through an economical model of return times of investing into solar panels (Fath *et al.*, 2015).

Acknowledgments

We thank the anonymous reviewers whose comments improved the quality of the manuscript. We are grateful to Marko Gulin (University of Zagreb), Parag Wate and Volker Coors (University of Applied Sciences Stuttgart), and Paula Redweik (University of Lisbon) for their help while developing the software prototype. Further, we are thankful to the developers of the libraries which have been used: Nathan Charles (Solpy), Elwood C. Downey (XEphem), and Brandon Rhodes (PyEphem).

This research is supported by the Dutch Technology Foundation STW, which is part of the Netherlands Organisation for Scientific Research (NWO), and which is partly funded by the Ministry of Economic Affairs (project code: 11300).

References

Aarsen, R., *et al.*, 2015. Installed base registration of decentralised solar panels with applications in crisis management. *In*: *ISPRS Archives. Proceedings of the 10th International Conference on Geo-information for Disaster Management GI4DM*, Oct.., Montpellier, France.

Alam, N., Coors, V., and Zlatanova, S., 2013. Detecting shadow for direct radiation using CityGML models for photovoltaic potentiality analysis. *In*: C. Ellul, S. Zlatanova, M. Rumor and R. Laurini, eds. *Urban and Regional Data Management*. CRC Press, 191–196.

Arbia, G., Griffith, D., and Haining, R., 1998. Error propagation modelling in raster GIS: overlay operations. *International Journal of Geographical Information Science*, 12 (2), 145–167.

Arroyo Ohori, K., *et al.*, 2015a. Modeling a 3D City Model and Its Levels of Detail as a True 4D Model. *ISPRS International Journal of Geo-Information*, 4 (3), 1055–1075.

Arroyo Ohori, K., Ledoux, H., and Stoter, J., 2015b. A dimension-independent extrusion algorithm using generalised maps. *International Journal of Geographical Information Science*, In press, available online.

Bartie, P., *et al.*, 2010. Advancing visibility modelling algorithms for urban environments. *Computers, Environment and Urban Systems*, 34 (6), 518–531.

Baumanns, K. and Löwner, M.O., 2009. Refined estimation of solar energy potential on roof areas using decision trees on CityGML-data. *In*: *Geophysical Research Abstracts. EGU General Assembly*, Apr.., Vienna, Austria, p. 14044.

Bayod-Rújula, A.A., Ortego-Bielsa, A., and Martínez-Gracia, A., 2011. Photovoltaics on flat roofs: Energy considerations. *Energy*, 36 (4), 1996–2010.

Beekhuizen, J., *et al.*, 2014. Impact of input data uncertainty on environmental exposure assessment models: A case study for electromagnetic field modelling from mobile phone base stations. *Environmental Research*, 135, 148–155.

Behrens, T.E.J., *et al.*, 2003. Characterization and propagation of uncertainty in diffusion-weighted MR imaging. *Magnetic Resonance in Medicine*, 50 (5), 1077–1088.

Ben Fekih Fradj, N. and Löwner, M.O., 2012. Abschätzung des nutzbaren Dachflächenanteils für Solarenergie mit CityGML-Gebäudemodellen und Luftbildern. *In*: M.O. Löwner, F. Hillen and R. Wohlfahrt, eds. *Geoinformatik 2012 "Mobilität und Umwelt". Konferenzband zur Tagung Geoinformatik*, Mar.., Braunschweig, Germany, 171–177.

Ben-Haim, G., Dalyot, S., and Doytsher, Y., 2014. Local Absolute Vertical Accuracy Computation of Wide-Coverage Digital Terrain Models. *In*: *Proceedings of Joint International Conference on Geospatial Theory, Processing, Modelling and Applications*, Oct.., Toronto, Canada, 136–152.

Beneš, J., Wilkie, A., and Křivánek, J., 2014. Procedural Modelling of Urban Road Networks. *Computer Graphics Forum*, 33 (6), 132–142.

Besuievsky, G. and Patow, G., 2013. Customizable LoD for Procedural Architecture. *Computer Graphics Forum*, 32 (8), 26–34.

Biljecki, F., Ledoux, H., and Stoter, J., 2014a. Error propagation in the computation of volumes in 3D city models with the Monte Carlo method. *In*: S. Li and S. Dragicevic, eds. *ISPRS Annals. Proceedings of the ISPRS/IGU Joint International Conference on Geospatial Theory, Processing, Modelling and Applications*, Oct.., Toronto, Canada, 31–39.

Biljecki, F., Ledoux, H., and Stoter, J., 2014b. Height references of CityGML LOD1 buildings and their influence on applications. *In*: M. Breunig, A.D. Mulhim, E. Butwilowski, P.V. Kuper, J. Benner and K.H. Häfele, eds. *Proceedings of the 9th 3DGeoInfo Conference 2014*, Nov.., Dubai, UAE.

Biljecki, F., Ledoux, H., and Stoter, J., 2015a. An improved LOD specification for 3D building models and its CityGML realisation with the Random3Dcity procedural modelling engine. *Computers, Environment and Urban Systems*, Under review.

Biljecki, F., Ledoux, H., and Stoter, J., 2015b. Improving the consistency of multi-LOD CityGML datasets by removing redundancy. *In*: M. Breunig, A.D. Mulhim, E. Butwilowski, P.V. Kuper, J. Benner and K.H. Häfele, eds. *Lecture Notes in Geoinformation and Cartography. 3D Geoinformation Science*. Dubai, UAE: Springer International Publishing, 1–17.

Biljecki, F., *et al.*, 2014c. Formalisation of the level of detail in 3D city modelling. *Computers, Environment and Urban Systems*, 48, 1–15.

Biljecki, F., *et al.*, 2013. Revisiting the concept of level of detail in 3D city modelling. *In*: U. Isikdag, ed. *ISPRS Annals. Proceedings of the ISPRS 8th 3D GeoInfo Conference & WG II/2 Workshop*, Nov.., Istanbul, Turkey, 63–74.

Boeters, R., *et al.*, 2015. Automatically enhancing CityGML LOD2 models with a corresponding indoor geometry. *International Journal of Geographical Information Science*.

Brenner, C., 2005. Building reconstruction from images and laser scanning. *International Journal of Applied Earth Observation and Geoinformation*, 6 (3-4), 187–198.

Bretagnon, P. and Francou, G., 1988. Planetary theories in rectangular and spherical variables. VSOP 87 solutions. *Astronomy and Astrophysics*, 202, 309–315.

Brown, J.D. and Heuvelink, G.B.M., 2007. The Data Uncertainty Engine (DUE): A software tool for assessing and simulating uncertain environmental variables. *Computers and Geosciences*, 33 (2), 172–190.

Burnicki, A.C., Brown, D.G., and Goovaerts, P., 2007. Simulating error propagation in land-cover change analysis: The implications of temporal dependence. *Computers, Environment and Urban Systems*, 31 (3), 282–302.

Carneiro, C. and Golay, F., 2009. Solar Radiation over the Urban Texture: LIDAR Data and Image Processing Techniques for Environmental Analysis at City Scale. *In*: J. Lee and S. Zlatanova, eds. *3D Geo-Information Sciences*. Berlin, Heidelberg: Springer Berlin Heidelberg, 319–340.

Caspary, W. and Scheuring, R., 1993. Positional accuracy in spatial databases. *Computers, Environment and Urban Systems*, 17 (2), 103–110.

Catita, C., *et al.*, 2014. Extending solar potential analysis in buildings to vertical facades. *Computers and Geosciences*, 66, 1–12.

Christensen, C.B. and Barker, G.M., 2001. Effects of tilt and azimuth on annual incident solar radiation for United States locations. *In*: *Proceedings of Solar Forum 2001: Solar Energy: The Power to Choose*, Apr.., Washington, DC, United States, 1–8.

Chwieduk, D.A., 2009. Recommendation on modelling of solar energy incident on a building envelope. *Renewable Energy*, 34 (3), 736–741.

D'Agostino, R.B., 1971. An omnibus test of normality for moderate and large size samples. *Biometrika*, 58 (2), 341–348.

David, M., Lauret, P., and Boland, J., 2013. Evaluating tilted plane models for solar radiation using comprehensive testing procedures, at a southern hemisphere location. *Renewable Energy*, 51 (C), 124–131.

Davis, T.J. and Keller, C.P., 1997. Modelling uncertainty in natural resource analysis using fuzzy sets and Monte Carlo simulation: slope stability prediction. *International Journal of Geographical Information Science*, 11 (5), 409–434.

de Bruin, S., Heuvelink, G.B.M., and Brown, J.D., 2008. Propagation of positional measurement errors to agricultural field boundaries and associated costs. *Computers and Electronics in Agriculture*, 63 (2), 245–256.

Demain, C., Journée, M., and Bertrand, C., 2013. Evaluation of different models to estimate the global solar radiation on inclined surfaces. *Renewable Energy*, 50 (c), 710–721.

Donkers, S., *et al.*, 2015. Automatic conversion of IFC datasets to geometrically and semantically correct CityGML LOD3 buildings. *Transactions in GIS*, In press.

Eicker, U., *et al.*, 2015. Energy performance assessment in urban planning competitions. *Applied Energy*, 155, 323–333.

Eicker, U., *et al.*, 2014. Assessing Passive and Active Solar Energy Resources in Cities Using 3D City Models. *Energy Procedia*, 57, 896–905.

Emmi, P.C. and Horton, C.A., 1995. A Monte Carlo simulation of error propagation in a GIS-based assessment of seismic risk. *International Journal of Geographical Information Science*, 9 (4), 447–461.

Fan, L., *et al.*, 2014. Propagation of vertical and horizontal source data errors into a TIN with linear interpolation. *International Journal of Geographical Information Science*, 28 (7), 1378–1400.

Fath, K., *et al.*, 2015. A method for predicting the economic potential of (building-integrated) photovoltaics in urban areas based on hourly Radiance simulations. *Solar Energy*, 116, 357–370.

Fischer, A., *et al.*, 1998. Extracting Buildings from Aerial Images Using Hierarchical Aggregation in 2D and 3D. *Computer Vision and Image Understanding*, 72 (2), 185–203.

Fisher, P.F., 1991. Modelling soil map-unit inclusions by Monte Carlo simulation. *International Journal of Geographical Information Science*, 5 (2), 193–208.

Fisher, P.F., 2005. Models of uncertainty in spatial data. *In*: P.A. Longley, M.F. Goodchild, D.J. Maguire and D.W. Rhind, eds. *Geographical Information Systems. Principles, Techniques, Management and Applications*. Wiley, 191–205.

Freitas, S., *et al.*, 2015. Modelling solar potential in the urban environment: State-of-the-art review. *Renewable and Sustainable Energy Reviews*, 41, 915–931.

Goetz, M., 2013. Towards generating highly detailed 3D CityGML models from OpenStreetMap. *International Journal of Geographical Information Science*, 27 (5), 845–865.

Goodchild, M.F., 1991. Issues of quality and uncertainty. *In*: J.C. Muller, ed. *Advances in cartography*. Elsevier, 113–139.

Gooding, J., Crook, R., and Tomlin, A.S., 2015. Modelling of roof geometries from low-resolution LiDAR data for city-scale solar energy applications using a neighbouring buildings method. *Applied Energy*, 148, 93–104.

Gosselin, P.H. and Cord, M., 2006. Feature-based approach to semi-supervised similarity learning. *Pattern Recognition*, 39 (10), 1839–1851.

Gröger, G. and Plümer, L., 2012. CityGML – Interoperable semantic 3D city models. *ISPRS Journal of Photogrammetry and Remote Sensing*, 71, 12–33.

Gruber, G., Menard, C., and Schachinger, B., 2008. Evaluation of the Geometric Accuracy of Automatically Recorded 3D – City Models Compared to GIS-Data. *The European Information Society*. Berlin, Heidelberg: Springer Berlin Heidelberg, 67–78.

Gulin, M., Vašak, M., and Baotić, M., 2013a. Estimation of the global solar irradiance on tilted surfaces. *In*: *Proceedings of the 17th International Conference on Electrical Drives and Power Electronics (EDPE 2013)*, Oct.., Dubrovnik, Croatia, 334–339.

Gulin, M., Vašak, M., and Perić, N., 2013b. Dynamical optimal positioning of a photovoltaic panel in all weather conditions. *Applied Energy*, 108, 429–438.

Haala, N. and Kada, M., 2010. An update on automatic 3D building reconstruction. *ISPRS Journal of Photogrammetry and Remote Sensing*, 65 (6), 570–580.

Harwin, S. and Lucieer, A., 2012. Assessing the Accuracy of Georeferenced Point Clouds Produced via Multi-View Stereopsis from Unmanned Aerial Vehicle (UAV) Imagery. *Remote Sensing*, 4 (6), 1573–1599.

Helbich, M., *et al.*, 2013. Boosting the predictive accuracy of urban hedonic house price models through airborne laser scanning. *Computers, Environment and Urban Systems*, 39 (C), 81–92.

Hengl, T., Heuvelink, G.B.M., and van Loon, E.E., 2010. On the uncertainty of stream networks derived from elevation data: the error propagation approach. *Hydrology and Earth System Sciences*, 14 (7), 1153–1165.

Herbert, G. and Chen, X., 2014. A comparison of usefulness of 2D and 3D representations of urban planning. *Cartography and Geographic Information Science*, 42 (1), 22–32.

Heuvelink, G.B.M., 2005. Propagation of error in spatial modelling with GIS. *In*: P.A. Longley, M.F. Goodchild, D.J. Maguire and D.W. Rhind, eds. *Geographical Information Systems. Principles, Techniques, Management and Applications*. Wiley, 207–217.

Heuvelink, G.B.M., Brown, J.D., and van Loon, E.E., 2007. A probabilistic framework for representing and simulating uncertain environmental variables. *International Journal of Geographical Information Science*, 21 (5), 497–513.

Heuvelink, G.B.M. and Burrough, P.A., 1993. Error propagation in cartographic modelling using Boolean logic and continuous classification. *International Journal of Geographical Information Science*, 7 (3), 231–246.

Heuvelink, G.B.M., Burrough, P.A., and Stein, A., 1989. Propagation of errors in spatial modelling with GIS. *International Journal of Geographical Information Science*, 3 (4), 303–322.

Hofierka, J. and Kaňuk, J., 2009. Assessment of photovoltaic potential in urban areas using open-source solar radiation tools. *Renewable Energy*, 34 (10), 2206–2214.

Hofierka, J. and Zlocha, M., 2012. A New 3-D Solar Radiation Model for 3-D City Models. *Transactions in GIS*, 16 (5), 681–690.

Hong, S. and Vonderohe, A., 2014. Uncertainty and Sensitivity Assessments of GPS and GIS Integrated Applications for Transportation. *Sensors*, 14 (2), 2683–2702.

Huld, T., Müller, R., and Gambardella, A., 2012. A new solar radiation database for estimating PV performance in Europe and Africa. *Solar Energy*, 86 (6), 1803–1815.

INSPIRE Thematic Working Group Buildings, 2013. D2.8.III.2 INSPIRE Data Specification on Buildings – Technical Guidelines. [online] [????].

Isikdag, U. and Zlatanova, S., 2009. Towards Defining a Framework for Automatic Generation of Buildings in CityGML Using Building Information Models. *3D Geo-Information Sciences*. Berlin, Heidelberg: Springer Berlin Heidelberg, 79–96.

Jakubiec, J.A. and Reinhart, C.F., 2013. A method for predicting city-wide electricity gains from photovoltaic panels based on LiDAR and GIS data combined with hourly Daysim simulations. *Solar Energy*, 93, 127–143.

Jochem, A., *et al.*, 2009. Automatic Roof Plane Detection and Analysis in Airborne Lidar Point Clouds for Solar Potential Assessment. *Sensors*, 9 (7), 5241–5262.

Kaartinen, H., *et al.*, 2005. Accuracy of 3D city models: EuroSDR comparison. *In*: G. Vosselman and C. Brenner, eds. *ISPRS Annals. Proceedings of the ISPRS Workshop Laser scanning 2005*, Sep.., Enschede, the Netherlands, 227–232.

Kaden, R. and Kolbe, T.H., 2014. Simulation-Based Total Energy Demand Estimation of Buildings using Semantic 3D City Models. *International Journal of 3-D Information Modeling*, 3 (2), 35–53.

Kalogirou, S.A., 2003. Generation of typical meteorological year (TMY-2) for Nicosia, Cyprus. *Renewable Energy*, 28 (15), 2317–2334.

Kelly, T. and Wonka, P., 2011. Interactive architectural modeling with procedural extrusions. *ACM Transactions on Graphics*, 30 (2), 1–15.

Kolbe, T.H., 2009. Representing and exchanging 3D city models with CityGML. *In*: S. Zlatanova and J. Lee, eds. *3D Geo-Information Sciences*. Springer Berlin Heidelberg, 15–31.

Kumar, L., Skidmore, A.K., and Knowles, E., 1997. Modelling topographic variation in solar radiation in a GIS environment. *International Journal of Geographical Information Science*, 11 (5), 475–497.

Ledoux, H. and Meijers, M., 2011. Topologically consistent 3D city models obtained by extrusion. *International Journal of Geographical Information Science*, 25 (4), 557–574.

Leica, 2008. Leica ALS70-CM City Mapping Airborne LIDAR Product Specifications. *leica-geosystems.us*.

Lemmens, M., 2011. Quality of Geo-information. *Geo-information. Technologies, Applications and the Environment*. Dordrecht: Springer Netherlands, 211–227.

Li, Y., Brimicombe, A.J., and Ralphs, M.P., 2000. Spatial data quality and sensitivity analysis in GIS and environmental modelling: the case of coastal oil spills. *Computers, Environment and Urban Systems*, 24 (2), 95–108.

Li, Z., Zhang, Z., and Davey, K., 2015. Estimating Geographical PV Potential Using LiDAR Data for Buildings in Downtown San Francisco. *Transactions in GIS*, n/a–n/a.

Liang, J., *et al.*, 2014. A visualization-oriented 3D method for efficient computation of urban solar radiation based on 3D–2D surface mapping. *International Journal of Geographical Information Science*, 28 (4), 780–798.

Liang, J., *et al.*, 2015. An open-source 3D solar radiation model integrated with a 3D Geographic Information System. *Environmental Modelling & Software*, 64 (C), 94–101.

Loch-Dehbi, S. and Plümer, L., 2011. Automatic reasoning for geometric constraints in 3D city models with uncertain observations. *ISPRS Journal of Photogrammetry and Remote Sensing*, 66 (2), 177–187.

Lukač, N., *et al.*, 2013. Rating of roofs' surfaces regarding their solar potential and suitability for PV systems, based on LiDAR data. *Applied Energy*, 102, 803–812.

MacLeod, M., Fraser, A.J., and Mackay, D., 2002. Evaluating and expressing the propagation of uncertainty in chemical fate and bioaccumulation models. *Environmental Toxicology and Chemistry*, 21 (4), 700–709.

Mainzer, K., *et al.*, 2014. A high-resolution determination of the technical potential for residential-roof-mounted photovoltaic systems in Germany. *Solar Energy*, 105, 715–731.

Mardaljevic, J. and Rylatt, M., 2003. Irradiation mapping of complex urban environments: an image-based approach. *Energy and Buildings*, 35 (1), 27–35.

Masters, G.M., 2013. *Renewable and Efficient Electric Power Systems*. 2 Wiley-Interscience.

Meeus, J.H., 1998. *Astronomical Algorithms*. 2 Willmann-Bell, Incorporated.

Müller, P., *et al.*, 2006. Procedural modeling of buildings. *ACM Transactions on Graphics*, 25 (3), 614–623.

Musialski, P., *et al.*, 2013. A Survey of Urban Reconstruction. *Computer Graphics Forum*, 32 (6), 146–177.

Nguyen, H.T. and Pearce, J.M., 2012. Incorporating shading losses in solar photovoltaic potential assessment at the municipal scale. *Solar Energy*, 86 (5), 1245–1260.

Nouvel, R., *et al.*, 2013. CityGML-based 3D city model for energy diagnostics and urban energy policy support. *In*: *Proceedings of BS2013: 13th Conference of International Building Performance Simulation Association*, Aug.., Chambéry, France, 218–225.

Nouvel, R., *et al.*, 2014. Urban Energy Analysis Based on 3D City Model for National Scale Applications. *In*: *Proceedings of the Fifth German-Austrian IBPSA Conference (BauSIM 2014)*, Sep.., Aachen, Germany, 83–90.

Open Geospatial Consortium, 2012. OGC City Geography Markup Language (CityGML) Encoding Standard 2.0.0. [online] [????].

Oude Elberink, S. and Vosselman, G., 2011. Quality analysis on 3D building models reconstructed from airborne laser scanning data. *ISPRS Journal of Photogrammetry and Remote Sensing*, 66 (2), 157–165.

Perez, R., *et al.*, 1990. Modeling daylight availability and irradiance components from direct and global irradiance. *Solar Energy*, 44 (5), 271–289.

Qi, H., Qi, P., and Altinakar, M.S., 2013. GIS-Based Spatial Monte Carlo Analysis for Integrated Flood Management with Two Dimensional Flood Simulation. *Water Resources Management*, 27 (10), 3631–3645.

Reda, I. and Andreas, A., 2004. Solar position algorithm for solar radiation applications. *Solar Energy*, 76 (5), 577–589.

Redweik, P., Catita, C., and Brito, M., 2013. Solar energy potential on roofs and facades in an urban landscape. *Solar Energy*, 97, 332–341.

Rottensteiner, F., *et al.*, 2014. Results of the ISPRS benchmark on urban object detection and 3D building reconstruction. *ISPRS Journal of Photogrammetry and Remote Sensing*, 93, 256–271.

Rowlands, I.H., Kemery, B.P., and Beausoleil-Morrison, I., 2011. Optimal solar-PV tilt angle and azimuth: An Ontario (Canada) case-study. *Energy Policy*, 39 (3), 1397–1409.

Santos, T., *et al.*, 2014. Applications of solar mapping in the urban environment. *Applied Geography*, 51, 48–57.

Saran, S., *et al.*, 2015. CityGML at semantic level for urban energy conservation strategies. *Annals of GIS*, 21 (1), 27–41.

Shi, W., 1998. A generic statistical approach for modelling error of geometric features in GIS. *International Journal of Geographical Information Science*, 12 (2), 131–143.

Shi, W., Cheung, C.K., and Zhu, C., 2003. Modelling error propagation in vector-based buffer analysis. *International Journal of Geographical Information Science*, 17 (3), 251–271.

Shi, W., Li, Q.Q., and Zhu, C., 2005. Estimating the propagation error of DEM from higher-order interpolation algorithms. *International Journal of Remote Sensing*, 26 (14), 3069–3084.

Stoter, J., de Kluijver, H., and Kurakula, V., 2008. 3D noise mapping in urban areas. *International Journal of Geographical Information Science*, 22 (8), 907–924.

Strzalka, A., *et al.*, 2012. Large scale integration of photovoltaics in cities. *Applied Energy*, 93, 413–421.

Strzalka, A., *et al.*, 2011. 3D City modeling for urban scale heating energy demand forecasting. *HVAC&R Research*, 17 (4), 526–539.

Šúri, M. and Hofierka, J., 2004. A New GIS-based Solar Radiation Model and Its Application to Photovoltaic Assessments. *Transactions in GIS*, 8 (2), 175–190.

Šúri, M., Huld, T.A., and Dunlop, E.D., 2005. PV-GIS: a web-based solar radiation database for the calculation of PV potential in Europe. *International Journal of Sustainable Energy*, 24 (2), 55–67.

Šúri, M., *et al.*, 2007. Potential of solar electricity generation in the European Union member states and candidate countries. *Solar Energy*, 81 (10), 1295–1305.

Suveg, I. and Vosselman, G., 2004. Reconstruction of 3D building models from aerial images and maps. *ISPRS Journal of Photogrammetry and Remote Sensing*, 58 (3-4), 202–224.

Taylor, J.R., 1997. *An Introduction to Error Analysis*. The Study of Uncertainties in Physical Measurements University Science Books.

Thevenard, D.J. and Brunger, A.P., 2002. The development of typical weather years for international locations: Part I, algorithms. *ASHRAE Transactions*, 108, 376–383.

Tomljenovic, I., *et al.*, 2015. Building Extraction from Airborne Laser Scanning Data: An Analysis of the State of the Art. *Remote Sensing*, 7 (4), 3826–3862.

Tooke, T.R., *et al.*, 2011. Tree structure influences on rooftop-received solar radiation. *Landscape and Urban Planning*, 102 (2), 73–81.

Tsiliakou, E., Labropoulos, T., and Dimopoulou, E., 2014. Procedural Modeling in 3D GIS Environment. *International Journal of 3-D Information Modeling*, 3 (3), 17–34.

van Oort, P., *et al.*, 2005. A variance and covariance equation for area estimates with a geographic information system. *Forest Science*, 51 (4), 347–356.

Vanegas, C.A., *et al.*, 2012. Procedural Generation of Parcels in Urban Modeling. *Computer Graphics Forum*, 31 (2), 681–690.

Veregin, H., 2005. Data quality parameters. *In*: P.A. Longley, M.F. Goodchild, D.J. Maguire and D.W. Rhind, eds. *Geographical Information Systems. Principles, Techniques, Management and Applications*. John Wiley & Sons, Inc, 177–189.

Veregin, H., 1995. Developing and testing of an error propagation model for GIS overlay operations. *International Journal of Geographical Information Science*, 9 (6), 595–619.

Vermeulen, T., *et al.*, 2015. Urban layout optimization framework to maximize direct solar irradiation. *Computers, Environment and Urban Systems*, 51, 1–12.

Vosselman, G. and Dijkman, S., 2001. 3D building model reconstruction from point clouds and ground plans. *In*: *ISPRS Archives. Proceedings of the workshop on Land surface mapping and characterization using laser altimetry*, Oct.., Annapolis, Maryland, USA, 37–44.

Wagen, J.F. and Rizk, K., 2003. Radiowave propagation, building databases, and GIS: anything in common? A radio engineer's viewpoint. *Environment and Planning B: Planning and Design*, 30 (5), 767–787.

Wiginton, L.K., Nguyen, H.T., and Pearce, J.M., 2010. Quantifying rooftop solar photovoltaic potential for regional renewable energy policy. *Computers, Environment and Urban Systems*, 34 (4), 345–357.

Wittmann, H., *et al.*, 1997. Identification of roof areas suited for solar energy conversion systems. *Renewable Energy*, 11 (1), 25–36.

Wonka, P., *et al.*, 2003. Instant architecture. *ACM Transactions on Graphics*, 22 (3), 669–677.

Xue, J., Leung, Y., and Ma, J.H., 2015. High-order Taylor series expansion methods for error propagation in geographic information systems. *Journal of Geographical Systems*, 17 (2), 187–206.

Yaagoubi, R., *et al.*, 2015. HybVOR: A Voronoi-Based 3D GIS Approach for Camera Surveillance Network Placement. *ISPRS International Journal of Geo-Information*, 4 (2), 754–782.

Yang, H. and Lu, L., 2007. The Optimum Tilt Angles and Orientations of PV Claddings for Building-Integrated Photovoltaic (BIPV) Applications. *Journal of Solar Energy Engineering*, 129 (2), 253.

Yasumoto, S., *et al.*, 2012. Virtual city models for assessing environmental equity of access to sunlight: a case study of Kyoto, Japan. *International Journal of Geographical Information Science*, 26 (1), 1–13.

Yeh, A.G.o. and Li, X., 2006. Errors and uncertainties in urban cellular automata. *Computers, Environment and Urban Systems*, 30 (1), 10–28.

Ying, M., Jingjue, J., and Fulin, B., 2002. 3D-City Model supporting for CCTV monitoring system. *In*: *ISPRS Archives. Proceedings of the ISPRS Commission IV Symposium on Geospatial Theory, Processing and Applications*, Jul.., Ottawa, Canada, p. 4.

Yu, B., *et al.*, 2009. Investigating impacts of urban morphology on spatio-temporal variations of solar radiation with airborne LIDAR data and a solar flux model: a case study of downtown Houston. *International Journal of Remote Sensing*, 30 (17), 4359–4385.

Zhang, S., Li, X., and Chen, Y., 2015. Error assessment of grid-based direct solar radiation models. *International Journal of Geographical Information Science*, 1–25.

Zhang, W., *et al.*, 2014. 3D Building Roof Modeling by Optimizing Primitive's Parameters Using Constraints from LiDAR Data and Aerial Imagery. *Remote Sensing*, 6 (9), 8107–8133.

Zhou, G., *et al.*, 2003. Spatial probabilistic modeling of slope failure using an integrated GIS Monte Carlo simulation approach. *Engineering Geology*, 68 (3-4), 373–386.